Microstructure and Dry Sliding Wear Performance of Oxide Dispersion Strengthened Austenitic Stainless Steel

Babatunde Abiodun Obadele[1*], Matsobane Stephans Ramashala[2], and Peter Apata Olubambi[1]

[1] Department of Chemical Engineering, University of Johannesburg, Johannesburg, South Africa
[2] Department of Chemical, Metallurgical and Materials Engineering, Tshwane University of Technology, Pretoria, South Africa

The oxide dispersion strengthening (ODS) material are candidates for structural materials in nuclear reactors due to high density of small oxide particles dispersed in the matrix. In this study, the microstructure and wear performance of ZrO_2 stabilized with Y_2O_3 reinforced AISI 316L austenitic stainless steels was investigated. The ODS-316L steel powders were sintered using spark plasma sintering technique. The surface structure and composition of the sintered samples were examined by field emission scanning electron microscopy (FESEM) equipped with energy dispersive spectroscopy (EDS) and X-ray diffraction (XRD). The experimental results were compared with the untreated 316L material. Tribological tests were performed on a ball-on-disc wear tester under dry condition at different applied loads from 5 to 35 N. The sliding distance was 2 mm for 1000 s. A tungsten carbide (WC) ball was used as a counterface material. Results showed that addition of ZrO_2 significantly improved the microhardness values while the presence of ZrO_2 phase in the 316L matrix reduces the friction coefficient and increased resistance to sliding wear.

INTRODUCTION

Powder metallurgy is an appropriate technique for the fabrication of composite materials. It comprises consolidating powder mixture by successive pressing and sintering or by hot pressing (Olmos et al., 2009). Stainless steels produced through powder technology route have found applications in mounting brackets for the rear view mirrors and the tone wheels for the antilock brake systems. These new sintered parts are being introduced newly in large amounts in produced cars (Dobrzański et al., 2007). The choice of stainless steel is due to the excellent resistance to corrosion and oxidation. However, stainless steels exhibit poor wear resistance. It has been extensively researched and established that the incorporation of hard, second-phase particles such as zirconia (an oxide dispersion strengthened (ODS) ceramic) deliberately added to ferrous matrices can significantly improve certain material properties such as wear and corrosion resistant (Obadele et al., 2013).

Oxide-dispersion-strengthened (ODS) stainless steels are the next generation materials in nuclear reactors and automotive parts. This is due to their outstanding strength, fatigue and creep properties as well as high irradiation resistance, thermomechanical stability and wear resistance (Darling et al., 2015, Hoelzer et al., 2007, Ukai and Fujiwara, 2002). ODS steels produced through powder metallurgy route has been reported to present excellent mechanical strength at high temperature (Li et al., 2010). Furthermore, it displays distinguished advantages both for high swelling resistance under heavy radiation and excellent corrosion and oxidation resistance (Hoelzer et al., 2007, Ukai et al., 2009).
This paper presents the results of researches carried out on the admixed ODS-316L austenitic stainless steels obtained by spark plasma sintering route and compared with 316L steel. This work has been focused towards the evaluation of influence of sintering parameters on the microstructure, hardness and dry wear behaviours of the sintered ODS-steel.

EXPERIMENTAL PROCEDURE

Materials

AISI 316 L stainless steel powder with an average particle size of 37 μm was selected as the matrix material. The nominal composition is presented in Table 1. ZrO_2 powder with an average particle size of 5 μm was used as the oxide dispersion strengthened reinforcement. The as-received powders were characterized for particle size distribution using a Malvern Mastersizer 2000 particle size analyzer (Microscientific) with water as a carrier fluid. The morphologies of the powders as well as their chemical compositions were analyzed using the field emission scanning electron microscope (FESEM) equipped with X-ray dispersive spectroscopy (EDS).

Table 1. Nominal composition for AISI 316L austenitic stainless steel

Sample	Cr	Ni	Mo	Si	Mn	N	Cu	S	P	C	Fe
AISI 316L	17.6	14.6	2.8	0.001	1.62	0.06	0.07	0.001	0.014	0.01	Bal.

Materials preparation

Prior to sintering, the 316L and ZrO_2 powders were mixed in different proportions in Turbula shaker mixer T2F as presented in Table 2. The two powders (316L and ZrO_2) were mixed at mixing speed of 49 rpm for 8 h in dry environment at room temperature. A 250 ml cylindrical plastic vessel with a fill level of 25% of the powders loaded axially was used. The mixing vessel is placed in the mixing chamber and subjected to translational and rotational motion. The mixing was varied at two-hour intervals for sampling. As the main objective of mixing is to produce a homogeneous feedstock with suitable rheological behavior for subsequent processing steps (Obadele et al., 2012), the homogeneity and possible bonding in the mixed powders were examined under field emission scanning electron microscope (FESEM) equipped with energy dispersive X-ray spectroscopy (EDS).

Table 2. Compositional Nominal composition for AISI 316L austenitic stainless steel

System	Powders	Vol. %
Substrate	AISI 316L	100
Sample 1	316L+ZrO_2	99:1
Sample 2	316L+ZrO_2	97:3
Sample 3	316L+ZrO_2	95:5

Spark plasma sintering

The mixed powders were sintered using HHPD-25 SPS System from FCT GmbH Germany in Ø20 mm graphite die. Graphite foils of 0.2 mm thickness were placed between the die and the powders for easy removal and significant reduction of temperature inhomogeneities. Sintering was performed in vacuum and a constant pressure was applied from the beginning of the heating step to the end of the dwell. The sintering parameters were: sintering temperature, 1100 °C; sintering pressure, 50 MPa; heating rate, 100 °C and holding time, 10 °C. When the required temperature and holding time was reached the electric current was shut off, the applied stress released, and the specimens were immediately cooled down in the furnace. Discs of 20 mm diameter of approximately 5 mm thickness were produced.

Density measurement and microstructural characterization

In order to measurement the density of the sintered samples, the samples were ground and polished to remove any surface graphite contamination. Afterward, the sintered density was determined by the Archimedes principle. The microstructure of the cross section of the samples were taken after polishing using SEM (FESEM, JSM-7600F, Jeol, Japan) equipped with with an EDS (Oxford X-Max)

with INCA X-Stream2 pulse analyzer software. The phases present in the sintered specimen were analysed by X-ray diffraction (XRD) using a PANalytical Empyrean model with Cu Kα radiation and analyzed using Highscore plus software. The XRD analysis was carried out on the section perpendicular to uniaxial pressed direction.

Microhardness

The hardness profile of the coated samples was measured using a Future-tech Vickers microhardness tester at a load 100 g (0.98 N) and dwell time of 15s. Indentations were taken at an interval of 100 mm. At each interval, ten indentations were taken and the average value was recorded..

Tribological test

In order to study the tribological behavior of the sintered samples (316L/+1%ZrO_2, +3%ZrO_2 and 5%ZrO_2), reciprocating–sliding friction tests were conducted using a CETRUMT-2 (Bruker Nano Inc., Campbell, CA) tribometer in a ball-on-disc configuration under ambient temperature. The test set up involved the use of a WC counterface ball sliding against the specimen in a reciprocating motion under different loads of 5, 15, 25 and 35 N and at a frequency of 5 Hz. Each test was repeated three times. The loads on the specimens were applied vertically downward with a motor-driven carriage that uses a load sensor for feedback to maintain a constant applied load. The dynamic normal load (FZ), friction force (Fx), depth of wear track (Z), and coefficient of friction (μ) were obtained from the UMT-2 tribometer software.

RESULTS AND DISCUSSION

As shown in Figure 1, SEM images of the powders are spherical and non-porous with fewer agglomeration. This suggests that the powders are prepared through gas atomization. EDS analysis of the powders also confirm the presence of desirable elements.

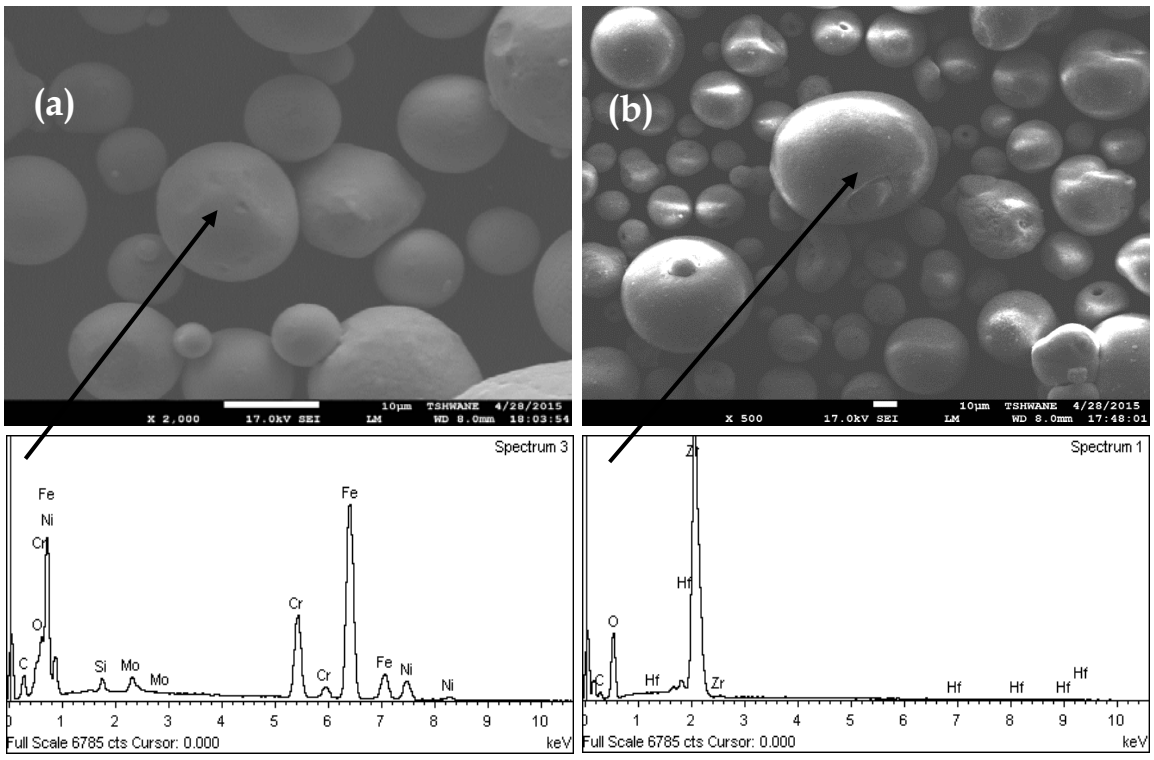

Figure 1. SEM/EDS images showing the morphology of (a) AISI 316L austenitic stainless steel and (b) Zirconia powders in as-received conditions

The effect of ZrO_2 addition on the final sintered density, and the results are shown in Figure 2. The measured relative density of the sintered 316L substrate was approximately 98%. As expected, the sintered density of 316L stainless steel samples decreased slightly with increase content of ZrO_2 additions. A maximum sintered relative density of 98% was achieved with 1% ZrO_2 addition. However, a decrease in density was measured at 3% and 5% ZrO_2 addition. This indicates that samples 2 and 3 are relatively porous when compared to sample 1. It is known that ZrO_2 addition in the matrix could have initiated the sintering process of the stainless steel powders by the formation of solid phase. The presence and increase content of this solid phase may result to formation of pores, thus reducing the sintered density. This could be seen in Figure 3, whereby, more pores are distributed in the matrix of 316L steel and around ZrO_2 particles. It is expected that at any given density, the densification rate is reduced with increasing volume fraction of reinforcements.

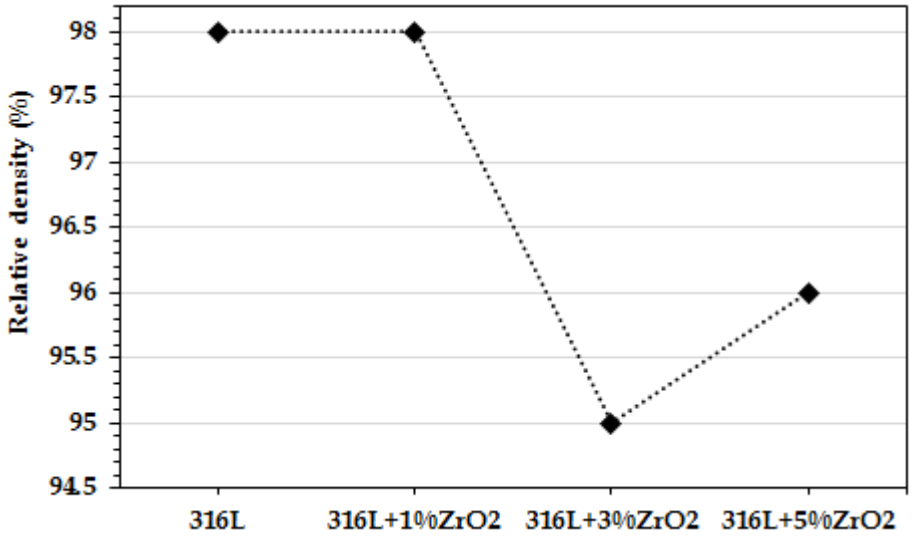

Figure 2. Effect of ZrO_2 addition on the sintering sintered relative density. Dots joining points are for visual aid only.

Figure 3 shows microstructure of sintered 316L stainless steel sample with various addition of ZrO_2 sintered at 1100 °C. Figure 3(b) shows the microstructure of samples with 1% ZrO_2, which exhibits sintered reinforced particles and without pore formation. Figure 3(c) and 3(d) show microstructure of samples with 3% and 5% ZrO_2 additions, respectively, in which sufficient amount of ZrO_2 solid phase is formed and 95-96% relative density was obtained. Unlike sample 1 (1% ZrO_2), sample 3 (5% ZrO_2) revealed the presence of pores. These pores in the neighbourhood of an inclusion are noticeably larger while no pores are visible within the 316L matrix.

The average microhardness values of the sintered samples showed an increasing trend from 340 $HV_{0.1}$ for sintered 316L steel to 437 $HV_{0.1}$ by increasing the content of ZrO_2 from 1% to 5%. Microhardness values of 388, 431 and 437 $HV_{0.1}$ were measured for samples 1, 2 and 3 respectively. It has been reported that the presence of ZrO_2 phase in composite matrix results in an increase in microhardness values (Obadele et al., 2015).

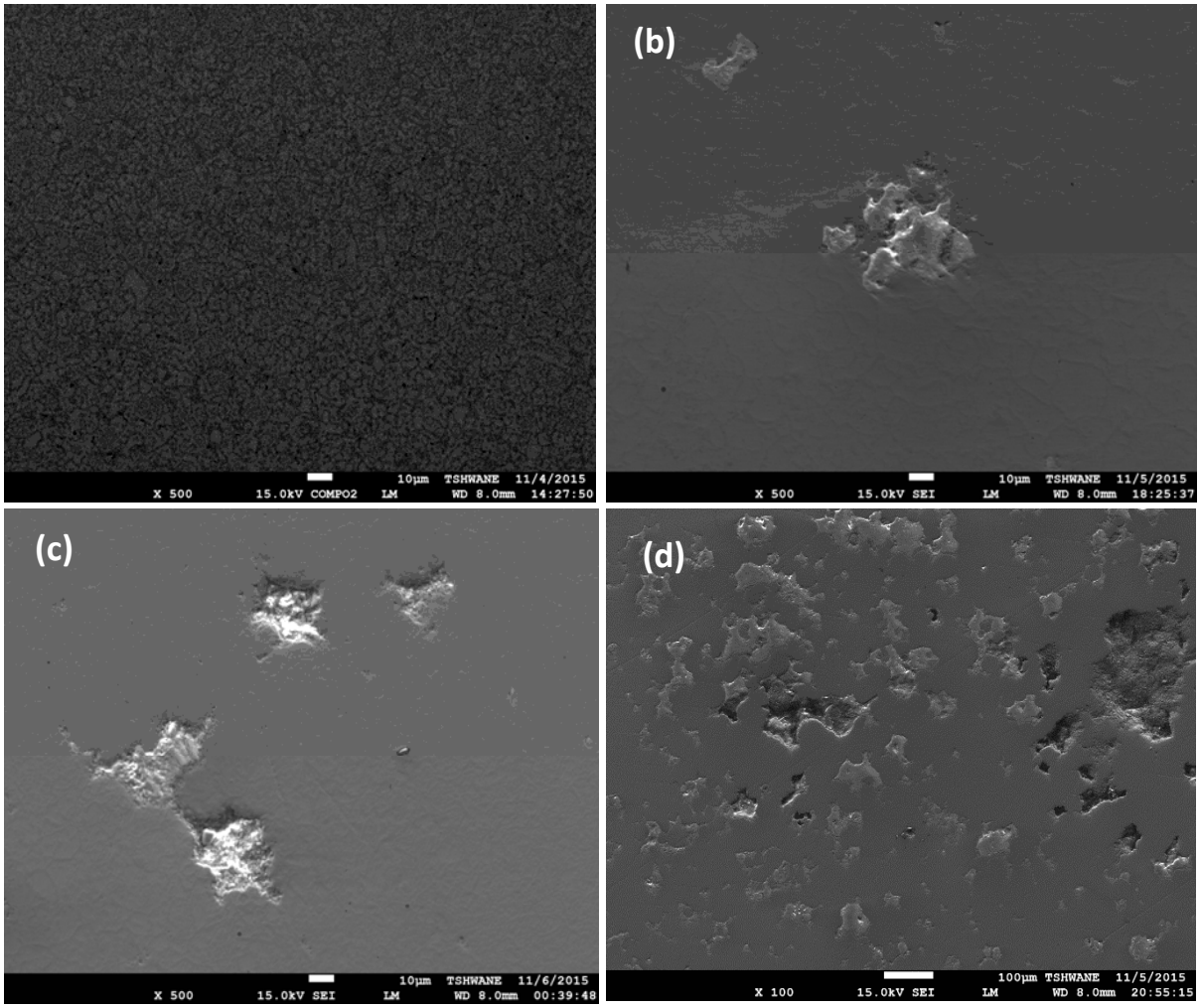

Figure 3. SEM micrographs of sintered (a) AISI 316L austenitic stainless steel with addition of (b) 1% ZrO_2, (c) 3% ZrO_2 and (d) 5% ZrO_2.

XRD
Figure 4

WEAR

Figure 5 shows the friction coefficient of 316L sintered substrate with various ZrO_2 additions under dry sliding conditions and different applied loads. It could be seen from Figure 5(a) that the friction coefficient of sintered 316L steel in the first 200 s varies at the different applied loads. At lower loads of 5 and 15 N, the friction coefficient increases steadily in the first 200 s followed by a sharp rise in friction coefficient. This sharp increase after 200 s could be attributed to the presence of third body within the worn track. This third body could accelerate the wear on the contact surface, thereby leading to delamination. Overall, the friction coefficient is between 0.5 and 0.6. The friction coefficient of sample 1 (Figure 5b) increases sharply at the onset of sliding time and reached a steady state afterwards until the load was removed. A slight reduction in the friction independent of content of Cu-lOSn alloy addition.

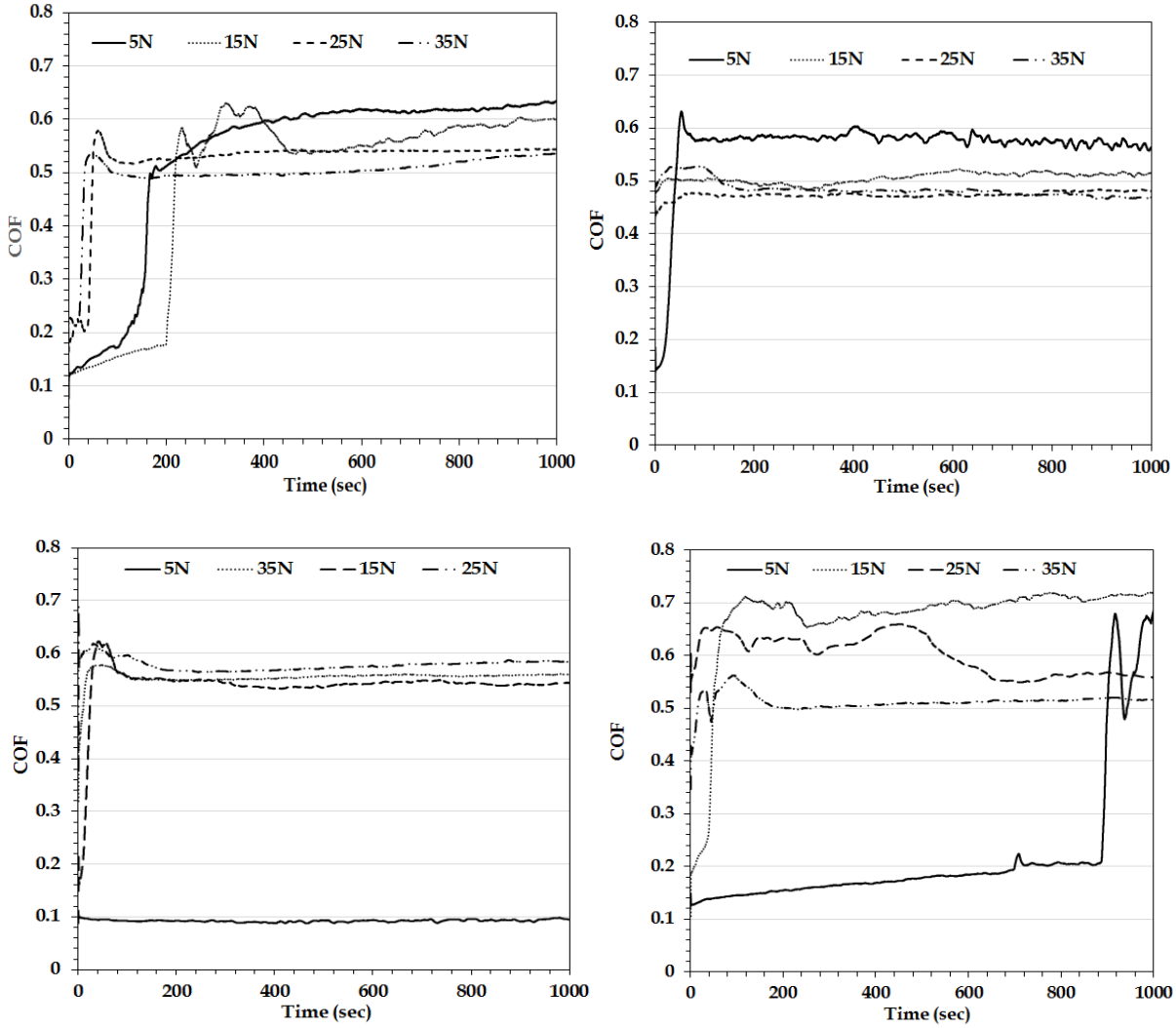

Figure 5. Variation of friction coefficients of (a) sintered 316L steel with (b) 1% ZrO_2, (c) 3% ZrO_2 and (d) 5% ZrO_2 under different applied loads of 5, 15, 25 and 35 N in dry condition.

DARLING, K. A., KAPOOR, M., KOTAN, H., HORNBUCKLE, B. C., WALCK, S. D., THOMPSON, G. B., TSCHOPP, M. A. & KECSKES, L. J. 2015. Structure and mechanical properties of Fe–Ni–Zr oxide-dispersion-strengthened (ODS) alloys. *Journal of Nuclear Materials,* 467, Part 1**,** 205-213.

DOBRZAŃSKI, L., BRYTAN, Z., GRANDE, M. A. & ROSSO, M. 2007. Influence of sintering parameters on the properties of duplex stainless steel. *Journal of Achievements in Materials and Manufacturing Engineering,* 20**,** 231-234.

HOELZER, D. T., BENTLEY, J., SOKOLOV, M. A., MILLER, M. K., ODETTE, G. R. & ALINGER, M. J. 2007. Influence of particle dispersions on the high-temperature strength of ferritic alloys. *Journal of Nuclear Materials,* 367–370, Part A**,** 166-172.

LI, M., ZHOU, Z., HE, P., LIAO, L., XU, Y. & GE, C. 2010. Microstructure and mechanical property of 12Cr oxide dispersion strengthened ferritic steel for fusion application. *Fusion Engineering and Design,* 85**,** 1573-1576.

OBADELE, B. A., ANDREWS, A., OLUBAMBI, P. A., MATHEW, M. T. & PITYANA, S. 2015. Effect of ZrO2 addition on the dry sliding wear behavior of laser clad Ti6Al4V alloy. *Wear,* 328–329**,** 295-300.

OBADELE, B. A., MASUKU, Z. H. & OLUBAMBI, P. A. 2012. Turbula mixing characteristics of carbide powders and its influence on laser processing of stainless steel composite coatings. *Powder Technology,* 230**,** 169-182.

OBADELE, B. A., OLUBAMBI, P. A. & JOHNSON, O. T. 2013. Effects of TiC addition on properties of laser particle deposited WC–Co–Cr and WC–Ni coatings. *Transactions of Nonferrous Metals Society of China,* 23**,** 3634-3642.

OLMOS, L., MARTIN, C. L. & BOUVARD, D. 2009. Sintering of mixtures of powders: Experiments and modelling. *Powder Technology,* 190**,** 134-140.

UKAI, S. & FUJIWARA, M. 2002. Perspective of ODS alloys application in nuclear environments. *Journal of Nuclear Materials,* 307–311, Part 1**,** 749-757.

UKAI, S., OHTSUKA, S., KAITO, T., SAKASEGAWA, H., CHIKATA, N., HAYASHI, S. & OHNUKI, S. 2009. High-temperature strength characterization of advanced 9Cr-ODS ferritic steels. *Materials Science and Engineering: A,* 510–511**,** 115-120.